Parametric model of the Mueller matrix of a Spectralon white reflectance standard deduced by polar decomposition techniques

Morten Kildemo,* Jérôme Maria, Pål G. Ellingsen, and Lars M. S. Aas

Department of Physics, The Norwegian University of Science and Technology (NTNU), N-7491 Trondheim, Norway

**Morten.Kildemo@ntnu.no*

Abstract: Decomposition methods have been applied to in-plane Mueller matrix ellipsometric scattering data of the Spectralon reflectance standard. Data were measured at the wavelengths 532 nm and 1500 nm, using an achromatic optimal Mueller matrix scatterometer applying a photomultiplier tube and a high gain InGaAs detector for the two wavelengths. A parametric model with physical significance was deduced through analysis of the product decomposed matrices. It is found that when the data are analyzed as a function of the scattering angle, similar to particle scattering, the matrix elements are largely independent of incidence angle. To the first order, we propose that a Guassian lineshape is appropriate to describe the polarization index, while the decomposed diagonal elements of the retardance matrix have a form resembling Rayleigh single scattering. New models are proposed for the off diagonal elements of the measured Mueller matrix.

OCIS codes: (120.2130) Ellipsometry and polarimetry; (290.5820) Scattering measurements; (290.5855) Scattering, polarization; (290.1350) Backscattering; (290.1990) Diffusion.

References and links

1. Ø. Svensen, M. Kildemo, J. Maria, J. J. Stamnes, and Ø. Frette, "Mueller matrix measurements and modeling pertaining to spectralon white reflectance standards," Opt. Express **20**, 15045–15053 (2012).
2. T. A. Germer and H. J. Patrick, "Mueller matrix bidirectional reflectance distribution function measurements and modeling of diffuse reflectance standards," Proc. SPIE **8160**, 81600D (2011).
3. D. A. Haner, B. T. McGuckin, and C. J. Bruegge, "Polarization characteristics of spectralon illuminated by coherent light," Appl. Opt. **38**, 6350–6356 (1999).
4. A. Bhandari, B. Hamre, Ø. Frette, L. Zhao, J. J. Stamnes, and M. Kildemo, "Bidirectional reflectance distribution function of spectralon white reflectance standard illuminated by incoherent unpolarized and plane-polarized light," Appl. Opt. **50**, 2431–2442 (2011).
5. T. A. Leskova, P. A. Letnes, A. A. Maradudin, T. Nordam, and I. Simonsen, "The scattering of light from two-dimensional randomly rough surfaces," Proc. SPIE **8172**, 817208 (2011).
6. I. Simonsen, A. A. Maradudin, and T. A. Leskova, "Scattering of electromagnetic waves from two-dimensional randomly rough penetrable surfaces," Phys. Rev. Lett. **104**, 223904 (2010).
7. I. Simonsen, A. A. Maradudin, and T. A. Leskova, "Scattering of electromagnetic waves from two-dimensional randomly rough perfectly conducting surfaces: The full angular intensity distribution," Phys. Rev. A **81**, 013806 (2010).
8. N. Ghosh, J. Soni, M. Wood, M. Wallenberg, and I. Vitkin, "Mueller matrix polarimetry for the characterization of complex random medium like biological tissues," Pramana **75**, 1071–1086 (2010).

#188283 - $15.00 USD Received 11 Apr 2013; revised 11 Jul 2013; accepted 11 Jul 2013; published 26 Jul 2013

9. N. Ghosh and I. A. Vitkin, "Tissue polarimetry: concepts, challenges, applications, and outlook," J. Biomed. Opt. **16**, 110801 (2011).
10. A. Pierangelo, S. Manhas, A. Benali, M. R. Antonelli, T. Novikova, P. Validire, B. Gayet, and A. De Martino, "Use of mueller polarimetric imaging for the staging of human colon cancer," Proc. SPIE **7895**, 78950E (2011).
11. V. V. Tuchin, L. V. Wang, and D. A. Zimnyakov, *Optical Polarization in Biomedical Applications* (Berlin Heidelberg, 2006).
12. S. Kumar, H. Purwar, R. Ossikovski, I. A. Vitkin, and N. Ghosh, "Comparative study of differential matrix and extended polar decomposition formalisms for polarimetric characterization of complex tissue-like turbid media," Journal of Biomedical Optics **17**, 105006–105006 (2012).
13. R. Ossikovski, A. D. Martino, and S. Guyot, "Forward and reverse product decompositions of depolarizing mueller matrices," Opt. Lett. **32**, 689–691 (2007).
14. R. Ossikovski, M. Anastasiadou, S. Ben Hatit, E. Garcia-Caurel, and A. De Martino, "Depolarizing mueller matrices: how to decompose them?" Phys. Status Solidi (a) **205**, 720–727 (2008).
15. R. Ossikovski, "Analysis of depolarizing mueller matrices through a symmetric decomposition," J. Opt. Soc. Am. A **26**, 1109–1118 (2009).
16. R. Ossikovski, "Differential matrix formalism for depolarizing anisotropic media," Opt. Lett. **36**, 2330–2332 (2011).
17. S.-Y. Lu and R. A. Chipman, "Interpretation of mueller matrices based on polar decomposition," J. Opt. Soc. Am. A **13**, 1106–1113 (1996).
18. S. Manhas, M. K. Swami, P. Buddhiwant, N. Ghosh, P. K. Gupta, and J. Singh, "Mueller matrix approach for determination of optical rotation in chiral turbid media in backscattering geometry," Opt. Express **14**, 190–202 (2006).
19. N. Ortega-Quijano and J. L. Arce-Diego, "Mueller matrix differential decomposition." Opt. lett. **36**, 1942–4 (2011).
20. H. D. Noble and R. a. Chipman, "Mueller matrix roots algorithm and computational considerations." Opt. Express **20**, 17–31 (2012).
21. H. Noble, S. McClain, and R. Chipman, "Mueller matrix roots depolarization parameters," Appl. Optics **51**, 735–744 (2012).
22. C. Bohren and D. Huffman, *Absorption and Scattering of Light by Small Particles Interscience* (J. Wiley & Sons, New York, 1983).
23. P. Hauge, R. Muller, and C. Smith, "Conventions and formulas for using the mueller-stokes calculus in ellipsometry," Surf. Sci. **96**, 81 – 107 (1980).
24. R. Azzam and N. Bashara, *Ellipsometry and Polarized Light* (North Holland, 1977).
25. J. J. Gil and E. Bernabeu, "A depolarization criterion in mueller matrices," Opt. Acta **32**, 259–261 (1985).
26. S. R. Cloude, "Conditions for the physical realisability of matrix operators in polarimetry," Proc. SPIE **1166**, 177–185 (1989).
27. F. Stabo-Eeg, M. Kildemo, I. S. Nerbø, and M. Lindgren, "Well-conditioned multiple laser mueller matrix ellipsometer," Opt. Eng. **47**, 073604–073604–9 (2008).
28. R. Ossikovski, M. Anastasiadou, and A. D. Martino, "Product decompositions of depolarizing mueller matrices with negative determinants," Opt. Commun. **281**, 2406 – 2410 (2008).
29. R. L. White, "Polarization in reflection nebulae. I - Scattering properties of interstellar grains," Astrophys. J. **229**, 954–961 (1979).
30. A. Erbe, K. Tauer, and R. Sigel, "Ellipsometric light scattering for the characterization of thin layers on dispersed colloidal particles," Phys. Rev. E **73**, 031406 (2006).

1. Introduction

It is important to have a well characterized Mueller matrix of white reflectance standards, such as the Spectralon, in order to obtain correct measurements whenever applying this standard, and in particular, in cases where the polarization of light intervene in the measurement process [1–4]. For un-polarized and linearly polarized illumination, Spectralon white reflectance standards are well documented and often used as calibration standards for optical instruments, but for applications involving other polarization states, more documentation is needed [1]. The Spectralon is the commercial product closest to a Lambertian surface, and is a white diffuse material (based on polytetrafluoroethylene) with excellent reflection properties, produced by Labsphere, USA. It is formed as a thermoplastic resin by heat and pressure treatment. The thermoplastic materials are resin machined into flat, thermally stable, high permittivity surfaces with porosity within the top layer (generally a few tenths of a millimeter thick) that randomizes the phase of the incident light-due to internal multiple reflections-to produce diffuse reflected

#188283 - $15.00 USD Received 11 Apr 2013; revised 11 Jul 2013; accepted 11 Jul 2013; published 26 Jul 2013

light [4]. Indeed, the Spectralon has the highest diffuse reflectance values of any known substance (up to 99%) in the ultraviolet, visible, and near-infrared spectral ranges [1, 2], and the reflection properties are spectrally flat between 400 and 1500 nm.

It is further fundamentally interesting to understand how a scattering Mueller matrix from a strongly diffuse medium may be interpreted. It concerns both the interpretation of Mueller matrices resulting from rough surfaces [5–7], powder samples, or extremely diffuse materials such as the Spectralon [2], and the important related problem of Mueller matrices resulting from biological tissue, which has recently regained considerable interest [8–12]. A parametric model of the Mueller matrix elements of the Spectralon diffuser, which relates to basic physical phenomena within the diffuser appears useful in order to develop the understanding of other strongly scattering media, such as biological tissue.

Two recent studies by Svensen et al. [1] and Germer et al. [2] reported the Mueller matrix measurements of the Spectralon using the wavelengths 532 nm [1] and 632.8 nm [2]. In the work of Svensen et al., the Mueller matrix was presented for several incidence angles (0°, 30°, 45° and 60°), and it was shown that the Mueller matrix could to the first order be seen as the sum of an ideal diffuser and a correction matrix [1]. Furthermore, the degree of polarization was observed to be a key parameter in order to develop a parametric model for each of the elements of the Mueller matrix. The origin of the structure in the scattering Mueller matrix elements reported in the work of Svensen et al. was not found, but in a recent study by Germer et al. [2], it was noted that particle scattering is an important process for the Mueller matrix of the Spectralon. Therefore, we have here pursued the idea that the Mueller matrix of the Spectralon appears to belong to a more general class of particle scattering problems.

Considerable effort has been made in order to increase the understanding of the Mueller matrix using various decomposition methods [8,9,13–18]. Decomposition of the Mueller matrix allows to separate different polarization phenomena, and thus to identify the basic building blocks of a complicated Mueller matrix consisting of both dichroism, retardance and diffuse scattering [9]. In the current work, several decomposition methods have been applied to the in-plane Mueller matrix scattering measurements of the Spectralon. As a result, more detailed information about the sample has been extracted, and an improved parametric model for the Mueller matrix has been obtained. In particular, the parametric model was found by studying the data as a function of the Rayleigh scattering angle used in particle scattering experiments, and by using the basis functions revealed from the decomposition.

2. Decomposition theory and basis functions

Product or polar decomposition allows the decomposition of a Mueller matrix into a product of elementary Mueller matrices, describing depolarization, retardance and diattenuation [13,14,17]. However, a given product decomposition may not always be representing the physical phenomena taking place in the sample, particularly whenever the different polarization altering phenomena are randomly ordered or occur simultaneously. There are several possible product decomposition methods such as the symmetrical decomposition [15], and the more common forward [17] and reverse [13] decompositions which are strongly interrelated [13]. The differential decomposition [12, 16, 19] and the recently described roots decomposition [20, 21] are other possibly more appropriate alternatives. On the other hand, in the work of Svensen et al. [1], a simplified version of the sum (or spectral) decomposition [1, 14] was used to propose a parametrization of the Mueller matrix of the Spectralon.

In the Spectralon sample, many of the scattering phenomena that are altering the polarization, may be envisaged to occur simultaneously, and the imposed ordering of the polarizing phenomena in the product decomposition methods may be incorrect. As such, the forward, reverse and symmetrical polar decomposition are equally (un)valid. Unfortunately, the most natural decom-

#188283 - $15.00 USD Received 11 Apr 2013; revised 11 Jul 2013; accepted 11 Jul 2013; published 26 Jul 2013

position method for such a system, the differential decomposition method, is currently strictly only valid for transmission geometries. As a result, the application of a decomposition method is in this work regarded as an empirical mathematical method in order to enhance and reveal an underlying dominating trend in order to parametrize the optical response. We choose therefore to mainly report the application of the product decomposition, due to its numerical stability in the presence of noise, in order to reveal more information about the basis functions describing the scattering Mueller matrix elements.

The measured Mueller matrix ($\mathbf{M}$) is, in the forward polar decomposition, decomposed as [17]

$$\mathbf{M} = \mathbf{M}_\Delta \mathbf{M}_R \mathbf{M}_D, \tag{1}$$

where $\mathbf{M}_\Delta$ is the depolarization matrix, $\mathbf{M}_R$ is the retardance matrix, and $\mathbf{M}_D$ is the diattenuation matrix. In terms of the forward polar decomposition, the depolarization, retardance and diattenuation matrices are [17]

$$\mathbf{M}_\Delta = M_{11}\begin{bmatrix} 1 & \mathbf{0}^T \\ \mathbf{p} & \mathbf{m}_\Delta \end{bmatrix}, \qquad \mathbf{M}_D = \begin{bmatrix} 1 & \mathbf{d}^T \\ \mathbf{d} & \mathbf{m}_D \end{bmatrix}, \qquad \mathbf{M}_R = \begin{bmatrix} 1 & \mathbf{0}^T \\ \mathbf{0} & \mathbf{m}_R \end{bmatrix}. \tag{2}$$

The polarizance vector $\mathbf{p} = \begin{bmatrix} p_1 & p_2 & p_3 \end{bmatrix}^T$ and diattenuation vector $\mathbf{d} = \begin{bmatrix} d_1 & d_2 & d_3 \end{bmatrix}^T$ are directly available from the measured Mueller matrix, while the 3×3 submatrices $\mathbf{m}_\Delta$, $\mathbf{m}_R$ and $\mathbf{m}_D$ are determined by the polar decomposition formalism [13, 17]. For an ideal diffuser, the $\mathbf{M}_\Delta$ is diagonal and given by $M_{11}\cdot\mathrm{diag}(1,\alpha,\beta,\gamma)$, where α,β and γ quantify the degree of polarization of linear, elliptical and circular polarized light, respectively [14, 17]. However, in the work of Lu and Chipman [17] it was proposed that the eigenvalues of $\mathbf{m}_\Delta$ give the three principal depolarization factors, and hence the average degree of polarization can be defined by [17]

$$p_C = \frac{1}{3}(\alpha+\beta+\gamma). \tag{3}$$

The total retardance is calculated from the retardance matrix as [18]

$$R = \cos^{-1}\left(\frac{\mathrm{Tr}(\mathbf{M}_R)-1}{2}\right). \tag{4}$$

A non-depolarizing matrix can in many cases be made up of the basic building blocks of a diattenuator and a retarder. The block diagonal building block, the so-called isotropic dichroic retarder, commonly encountered in specular reflection from an isotropic surface, or from Mie scattering from small particles is a particularly useful reference

$$\mathbf{M}_{DR} = M_{11}\begin{bmatrix} 1 & m_{12} & 0 & 0 \\ m_{21} & 1 & 0 & 0 \\ 0 & 0 & m_{33} & m_{34} \\ 0 & 0 & m_{43} & m_{44} \end{bmatrix}. \tag{5}$$

For Mie spheres, expressions for the matrix elements are given by e.g. Bohren and Huffman [22], while for reflection from a plane isotropic surface, the matrix elements, for a $\{\hat{p},\hat{s},\hat{k}\}$ right handed geometry, are given by the normal ellipsometric angles Ψ and Δ [23, 24]

$$m_{12} = m_{21} = -\cos(2\Psi),\ m_{33} = m_{44} = \sin(2\Psi)\cos\Delta,\ m_{34} = -m_{43} = \sin(2\Psi)\sin\Delta. \tag{6}$$

For Rayleigh particles, the normalized Mueller matrix elements are further simplified and given by [22]

$$m_{12} = m_{21} = \frac{\sin^2(\theta_R)}{1+\cos^2(\theta_R)}, \qquad m_{33} = m_{44} = \frac{2\cos(\theta_R)}{1+\cos^2(\theta_R)}, \qquad m_{34} = m_{43} = 0. \tag{7}$$

#188283 - $15.00 USD Received 11 Apr 2013; revised 11 Jul 2013; accepted 11 Jul 2013; published 26 Jul 2013

The polarization index p_D (or degree of purity) [25], which is obtained from the full Mueller matrix was selected as the key figure to model the Spectralon Mueller matrix [1]

$$p_D = \left(\frac{\mathrm{Tr}\left(\mathbf{M}^T\mathbf{M}\right) - M_{11}^2}{3M_{11}^2} \right)^{1/2} = \left(\frac{\sum_{i,j=1}^{4} M_{ij}^2 - M_{11}^2}{3M_{11}^2} \right)^{1/2} . \tag{8}$$

The polarization index is between 0 and 1, i.e. $0 \leq p_D \leq 1$. When $p_D = 0$, the outgoing light is fully depolarized, and when $p_D = 1$, the outgoing light is fully polarized. This index compares well to the average degree of polarization p_c (Eq. (3)).

3. Experimental details

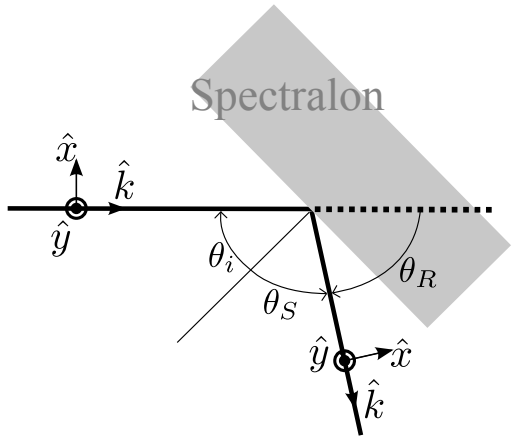

Fig. 1. Geometry for the scattering experiment, defining the incidence angle θ_i, the Rayleigh scattering angle θ_R and the Rayleigh scattering angle θ_S used in [1]. The figure also shows the right handed coordinate system $\{\hat{x},\hat{y},\hat{k}\}$ used in the paper, where $\hat{x} = -\hat{p}$, $\hat{y} = \hat{s}$ with reference to the right handed system $\{\hat{s},\hat{p},\hat{k}\}$. The arrows define positive direction.

New Mueller matrix data were recorded for the Spectralon in the in-plane scattering geometry shown in Fig. 1. The experimental data are presented according to the right handed coordinate system $\{\hat{x},\hat{y},\hat{k}\}$ where $\hat{x} = -\hat{p}$, $\hat{y} = \hat{s}$ with respect to the right handed system $\{\hat{s},\hat{p},\hat{k}\}$, see Fig. 1. All measurements were performed in the incidence plane (see Fig. 1 for the definitions of the angles). The Stokes vector is in this case given as

$$\mathbf{S} = \begin{bmatrix} I_{\hat{x}} + I_{\hat{y}} \\ I_{\hat{x}} - I_{\hat{y}} \\ I_{\hat{x}+\hat{y}} - I_{\hat{x}-\hat{y}} \\ I_{RC} - I_{LC} \end{bmatrix} . \tag{9}$$

Mueller matrices for an illumination wavelength of $\lambda = 532$ nm were measured at every 1° for scattering angles θ_S (see Fig. 1) relative to the normal of the Spectralon surface from -90° to 90°, with the exception of a dead-zone of $\pm 10^\circ$ around the back-scattering angle. A rotating diffuser was used prior to the polarization state generator in order to remove speckle effects [1].

#188283 - $15.00 USD Received 11 Apr 2013; revised 11 Jul 2013; accepted 11 Jul 2013; published 26 Jul 2013

Mueller matrices at $\lambda = 1500$ nm are reported for every 2° for θ_S from 10° to 90°, as we will show that the Mueller matrix was found similar to the one at $\lambda = 532$ nm. It is emphasized that the data at $\lambda = 1500$ may contain speckle effects, as no rotating diffuser was available for that wavelength. It is noted that all the measured Mueller matrices were found to be physical according to the Cloude filtering criterion [26].

A well conditioned broadband (achromatic) Mueller matrix ellipsometer [27] was used to acquire the experimental data at both wavelengths (see [1] for the experimental details at 532 nm). A 45 mW laser at 1500 nm and an InGaAs detector with variable gain $\left(10^5 - 10^9\right)$ were used for the near infrared measurement.

4. Results and discussion

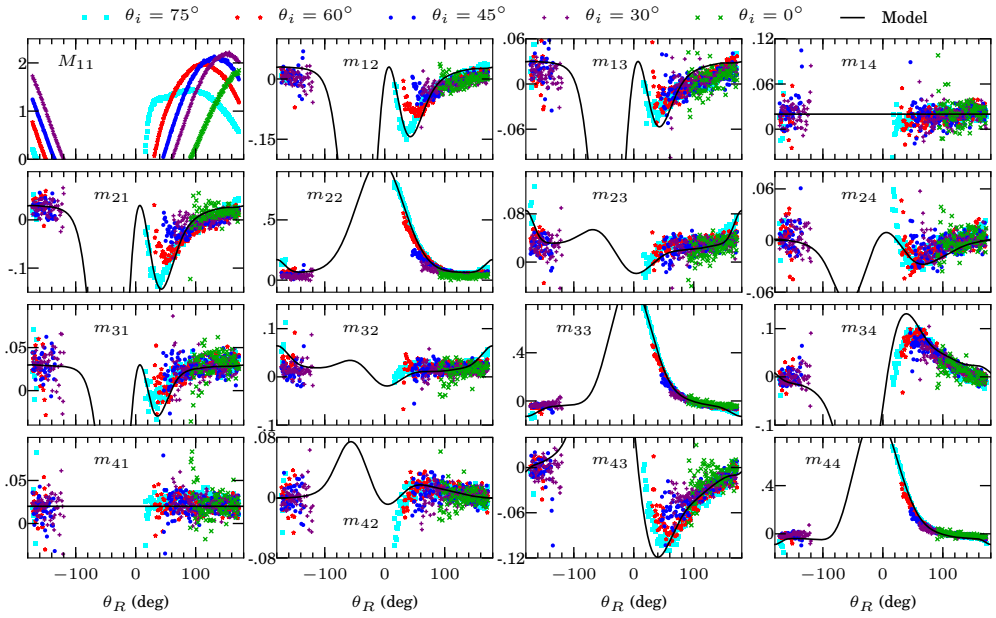

Fig. 2. The measured Mueller matrix data from the Spectralon surface with illumination at incidence angles θ_i of 0° (green x marks), 30° (purple crosses), 45° (blue circles), 60° (red stars), 75° (cyan squares) plotted as a function of the Rayleigh scattering angle θ_R. The full curves show the fitted parametric model in Eq. (19). All elements, except M_{11}, are normalized to M_{11}.

Figure 2 shows the Mueller matrices recorded at 532 nm for the angles of incidence 0°, 30°, 45°, 60° and 75°, where all elements have been normalized by M_{11}. The M_{11} element is proportional to the phase function, and is shown in the top left figure. Its form is typical for a near Lambertian diffuser [1,4], although the total intensity has not been calibrated in the current work. It is particularly noted that the Mueller matrix elements have been plotted and analyzed as a function of θ_R. It is observed from Fig. 2 that the general trend of the normalized Mueller matrix elements appears to be independent of the incidence angle. Deviations from this trend can be observed for light scattered nearly parallel to the sample surface. It is also observed that both block diagonal and off-block diagonal elements are non-zero, particularly for angles close to the sample surface, showing that the Spectralon in these cases is far from an ideal diffuser. The diagonal elements are seen to be strongly dominating for scattering near parallel to the

#188283 - $15.00 USD Received 11 Apr 2013; revised 11 Jul 2013; accepted 11 Jul 2013; published 26 Jul 2013

sample surface.

It is interesting to note that the amplitudes of the $m_{24} \approx -m_{42}$ elements oscillate with the azimuthal orientation (χ) of the sample (i.e. upon rotating the sample around its normal), and that they can be close to zero in a given orientation, see Fig. 3. Such an anisotropic effect was also observed by Germer et al. [2]. To demonstrate smaller variations in the remaining Mueller matrix elements upon sample rotation, we have also plotted $\Delta m_{33} \equiv m_{33} - \langle m_{33} \rangle$ and $\Delta(m_{34} - m_{43}) \equiv (m_{34} - \langle m_{34} \rangle) - (m_{43} - \langle m_{43} \rangle)$, where $\langle m_{ij} \rangle$ are the averages upon a full 360° rotation, as a function of χ. There may be a weak oscillation in the m_{34} and m_{43} elements, while the remaining elements are not observed to oscillate upon azimuthal rotation of the sample, similar to Δm_{33} in Fig. 3. It is thus curious that here the linear retardance between the ±45° axis is strongly oscillating, while the linear retardance along the $x-y$ axis is only weakly oscillating, when interpreted using the differential decomposition theory [12, 16]. However, the off-block diagonal elements are non-zero (except possibly m_{14} and m_{41}), although only m_{24} and m_{42} are observed to be sensitive to the azimuthal orientation of the sample (χ).

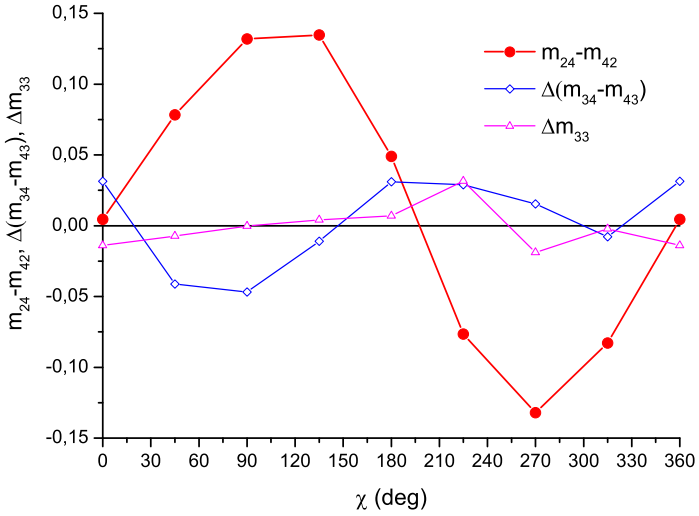

Fig. 3. The difference of the off-diagonal elements $(m_{24} - m_{42})$, $\Delta m_{33} \equiv m_{33} - \langle m_{33} \rangle$ and $\Delta(m_{34} - m_{43}) \equiv (m_{34} - \langle m_{34} \rangle) - (m_{43} - \langle m_{43} \rangle)$, where $\langle m_{ij} \rangle$ are the averages upon a full 360 degrees rotation, at 532 nm. The data are plotted against the azimuthal angle of the Spectralon for incidence angle 75° and Rayleigh scattering angle 35°.

Figure 4 shows the recorded Mueller matrix for both wavelengths 1500 nm and 532 nm for the angle of incidence 75°. The Mueller matrix at 1500 nm has a similar form, but with small differences that will be discussed below.

4.1. Model for p_D

When the data are plotted against the Rayleigh scattering angle, the depolarization indices p_D are also observed to become nearly independent of the incidence angles. Previously it was proposed that the following parametric model could represent the data [1]

$$p_D = \left| \frac{(\theta_S + \theta_i)^3}{22} \right| = \left| \frac{(180 - \theta_R)^3}{22} \right|. \tag{10}$$

#188283 - $15.00 USD Received 11 Apr 2013; revised 11 Jul 2013; accepted 11 Jul 2013; published 26 Jul 2013

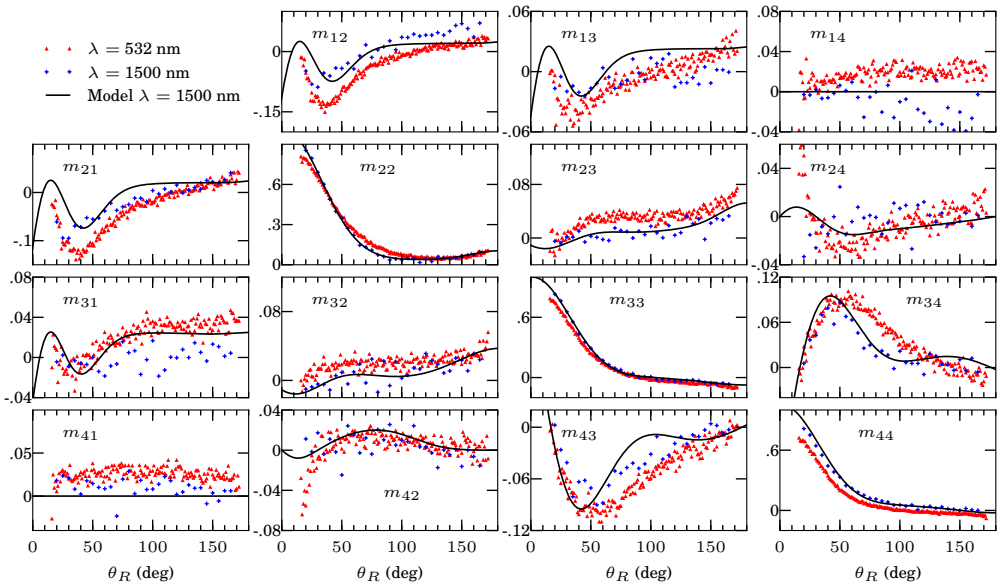

Fig. 4. Measured Mueller matrix data from the Spectralon surface with illumination at an incidence angle of $\theta_i = 75^\circ$ and wavelengths 532 nm (red triangles) and 1500 nm (blue crosses) plotted against the Rayleigh scattering angle θ_R. The full curve shows the fitted parametric model at 1500 nm in Eq. (19). All elements are normalized to M_{11}.

However, one may further argue that in the forward scattering direction, then both in the Mie and the Rayleigh scattering model, light should be highly polarized while p_D should be less or equal to one. This is also the case for scattering at a grazing incidence. Therefore, we propose that a peak function, such as the Gaussian function, is a more appropriate choice to fit the data, see Fig. 5. As a result, the following Gaussian function is proposed to model p_D

$$p_D(\theta_R) = p_0 + (1 - p_0 - p_{BS}) \exp\left(-0.5\left(\frac{\theta_R - \theta_F}{w_F}\right)^2\right) + p_{BS}(\theta_R), \tag{11}$$

where also a constant offset p_0 is added. Furthermore, a function p_{BS} is added in order to express the additional polarization taking place at the backscattering angle

$$p_{BS}(\theta_R) = A_{BS} \exp\left(-0.5\left(\frac{|\,\theta_R\,| - 180}{w_B}\right)^2\right). \tag{12}$$

The increased polarization at the backscattering angle is only weakly present in the data in Fig. 5, due to the design of the current Mueller matrix apparatus, but the data of Germer et al. confirm this trend [2]. It is clear that more structure in the data may be present at the backscattering angle. It is noted that the model is strictly only valid for $90^\circ - \theta_i \leq \theta_R$ and $\theta_R \leq -\theta_i - 90^\circ$. Furthermore, the model does not capture deviations in p_D for scattered light nearly parallel to the sample surface, as particularly seen from the data at 532 nm (Fig. 5(a)). Values for the fitted parameters for p_D on the entire data set at 532 nm are given in Table 1, and the plot is shown in Fig. 5(a).

#188283 - $15.00 USD Received 11 Apr 2013; revised 11 Jul 2013; accepted 11 Jul 2013; published 26 Jul 2013

A Gaussian lineshape was also observed for the p_D data at 1500 nm, as seen in Fig. 5(c) (note that data were here only recorded for positive θ_R). It shows that p_D from 532 nm (dashed line) is less polarized compared to 1500 nm (full line) for scattered light close to the surface plane. For the back scattering direction, 1500 nm is less polarized than 532 nm. Elsewhere, the differences appear small.

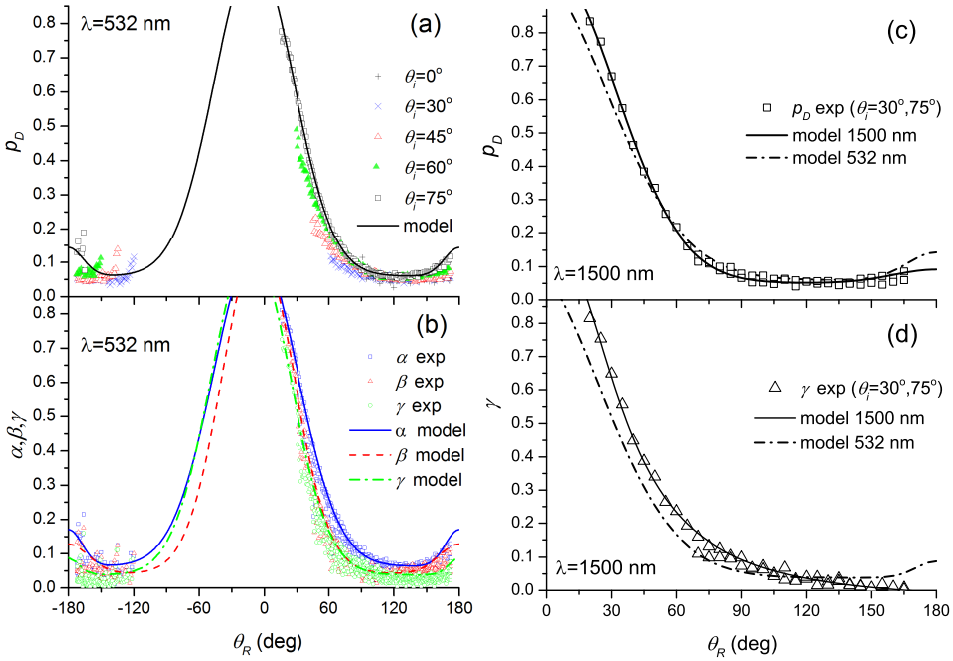

Fig. 5. Figures (a) and (b) show the depolarization index p_D (a) and the depolarization factors α, β and γ (b) determined from forward product decomposition for five different incidence angles ($\theta_i = 0°, 30°, 45°, 60°, 75°$) at λ =532 nm plotted against the Rayleigh scattering angle θ_R. Tentative fits are shown using the model in Eq. (11) and the parameters in Table 1. Figures (c) and (d) show the depolarization index p_D (c) and the depolarization factor γ (d) determined from the forward product decomposition for two different incidence angles ($\theta_i = 30°, 75°$) at $\lambda = 1500$ nm plotted against θ_R. The full and dotted lines in (c) show the fitted models for p_D to the data at $\lambda = 1500$ nm (see Table 2) and $\lambda = 532$ nm, respectively. The full and dotted lines in (d) shows the fitted model for γ in Eq. (13) with the parameters in Table 2 for $\lambda = 1500$ nm and the model for $\lambda = 532$ nm, respectively.

We will now develop an alternative parametric model for the Mueller matrices in Fig. 2 and in Fig. 4, by inspection of the decomposed Mueller matrices using the product decomposition, and looking for a mathematical form of the Mueller elements which may have a common physical interpretation. In particular, the forward polar decomposition allows to inspect the details of the retardance matrix $\mathbf{M}_R$, the diattenuation matrix $\mathbf{M}_D$ and the elements of the depolarization matrix $\mathbf{M}_\Delta$.

#188283 - $15.00 USD Received 11 Apr 2013; revised 11 Jul 2013; accepted 11 Jul 2013; published 26 Jul 2013

Table 1. Fitted parameters for the polarization index (p_D) and the depolarization factors, using Eq. (11) at 532 nm. The fitted data are shown in Figs. 5(a) and 5(b).

$\lambda = 532$ nm	p_0	w_F	$\theta_F(^\circ)$	A_{BS}	w_B
p_D	0.06	36.8	-9.4	0.08	13.4
α	0.06	38.6	-7.9	0.11	12.6
β	0.04	33.0	-5.7	0.086	18.5
γ	0.038	36.1	-12.4	0.05	9.4

4.2. Simplified model for $\boldsymbol{M}_\Delta$

The decomposed Mueller matrix was found to result in a close to diagonal $\mathbf{m}_\Delta$. The other off-diagonal elements were therefore for simplicity neglected in the analysis. Let us inspect these diagonal components which we then for simplicity relate directly to α, β and γ of the "diagonal" depolarization matrix at 532 nm (see Eq. (2)) in Fig. 5(b), where we also neglect the fact that we are not dealing with an ideal diffuser since the polarizance is non-zero [14]. The model in Eq. (11), was used to fit the full datasets for α, β and γ at 532 nm. The resulting parameters from the fits are given in Table 1. Again, it is noted that the parameters describing the back-scattering contribution are only indicative, since we have limited data in this region. The diagonal components α, β and γ of the depolarization matrix at 1500 nm involves another complication, as the measured matrix can be seen to change from a positive to a negative determinant as a function of the Rayleigh scattering angle. We have treated this issue using the recipe described by Ossikovski et al. [28]. However, we observe that at 1500 nm, γ has a different shape than at 532 nm, and at 1500 nm we had to use a Lorentzian peak function for a reasonable fit. As a result, the model in Eq. (11), was used to fit the full datasets for α, β at 1500 nm, while the following Lorentzian function was used to fit γ

$$p_0 + (1 - p_0)\left[1 + \left(\frac{\theta_R - \theta_F}{w_F}\right)^2\right]^{-1}. \tag{13}$$

The fitted parameters for α, β and γ for $\lambda = 1500$ nm are given in Table 2.

Table 2. Fitted parameters for the depolarization factors α and β using Eq. (11) and γ using Eq. (13), at 1500 nm. The fits to p_D and γ are shown in Fig. 5.

$\lambda = 1500$ nm	p_0	w_F	$\theta_F(^\circ)$	A_{BS}	w_B
p_D	0.05	31	1.2	0.04	20
α	0.037	31	2.8	0.067	22
β	0.011	31	1.7	0.06	35
γ	-0.04	32	6.7		

4.3. Simplified model for $\boldsymbol{M}_R$ and $\boldsymbol{M}_D$ matrices

Let us now analyze the retardance matrix, $\mathbf{M}_R$. First, inspecting the retardance in Eq. (4), one can observe a similar trend for the scattered light at 532 nm and at 1500 nm, see Fig. 6. In both cases, the retardance increases as a function of the Rayleigh scattering angle θ_R and crosses 90° after $\theta_R = 90^\circ$. There appears to be a definite observable difference between the two wavelengths. The jumps around $95^\circ - 110^\circ$ in the retardance at 1500 nm, are noise believed to be due to speckles.

#188283 - $15.00 USD Received 11 Apr 2013; revised 11 Jul 2013; accepted 11 Jul 2013; published 26 Jul 2013

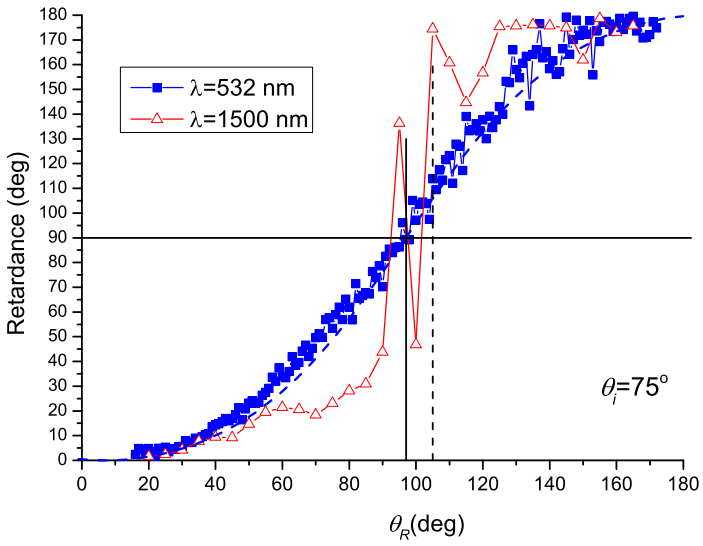

Fig. 6. Retardance (given by Eq. (4)) at 532 nm (full squares) and 1500 nm (hollow triangles) with incident angle $\theta_i = 75^\circ$ plotted as a function of the Rayleigh scattering angle θ_R. The two vertical lines indicate when the retardance crosses 90°. Note that θ_B (i.e. vertical lines) were determined from Fig. 7. The Figure also shows the function $R \approx \arccos(C)$ (blue dotted line), with $\theta_B \approx 7^\circ$.

Figures 7(a) and 7(c) shows the normalized m_{R33} and m_{R44} elements of the retardance matrix $\mathbf{M}_R$ for all recorded angles of incidence. Figs. 7(b) and 7(d) shows the retardance data of m_{R34} and m_{R43} for all recorded angles of incidence. It is interesting to observe that m_{R33} and m_{R44} are nearly identical and follow the Rayleigh scattering model for all incidence angles, when analyzed as a function of θ_R

$$C = m_{R33} = m_{R44} = \frac{2\cos(\theta_R - \theta_B)}{1+\cos^2(\theta_R - \theta_B)}, \tag{14}$$

except for an apparent shift of m_{R33} and m_{R44} of approximately $\theta_B \approx 7^\circ$ at 532 nm and $\theta_B \approx 15^\circ$ at 1500 nm as indicated by the vertical lines in Fig. 7. A similar functional form (without the shift) was used by White [29] and further proposed by Germer et al. [2] for modeling of the Spectralon. The shift θ_B, appears to be dispersive (i.e. a funtion of wavelength), although we find that a similar analysis of the Mueller matrix data reported by Germer et al. also gives a shift $\theta_B \approx 7^\circ$ at 632.8 nm. The shift θ_B is suggested related to a pseudo Brewster angle as a result of particle scattering [30]. It is also useful to observe that the total retardance R in Fig. 6 has a functional form well described by $R \approx \arccos(C)$, particularly at 532 nm.

The m_{R34} and m_{R43} elements, which are normally zero in the Rayleigh scattering model, are proposed to have a related form

$$S = m_{R34} = -m_{R43} = \frac{\sin(\theta_R - \theta_B)}{1+\cos^2(\theta_R - \theta_B)}, \tag{15}$$

with a similar shift of $\theta_B \approx 7^\circ$ at 532 nm and $\theta_B \approx 15^\circ$ at 1500 nm. The origin of such a functional form could be the averaging of the Mie scattering from anisotropic shaped particles. On the other hand, one could also imagine that light scattered by particles will travel through a

#188283 - $15.00 USD Received 11 Apr 2013; revised 11 Jul 2013; accepted 11 Jul 2013; published 26 Jul 2013

form-birefringent medium causing such a retardance. The retardance appears as the dominant effect, and its effect scales approximately with $p_D \approx \alpha \approx \beta \approx \gamma$ in the final Mueller matrix.

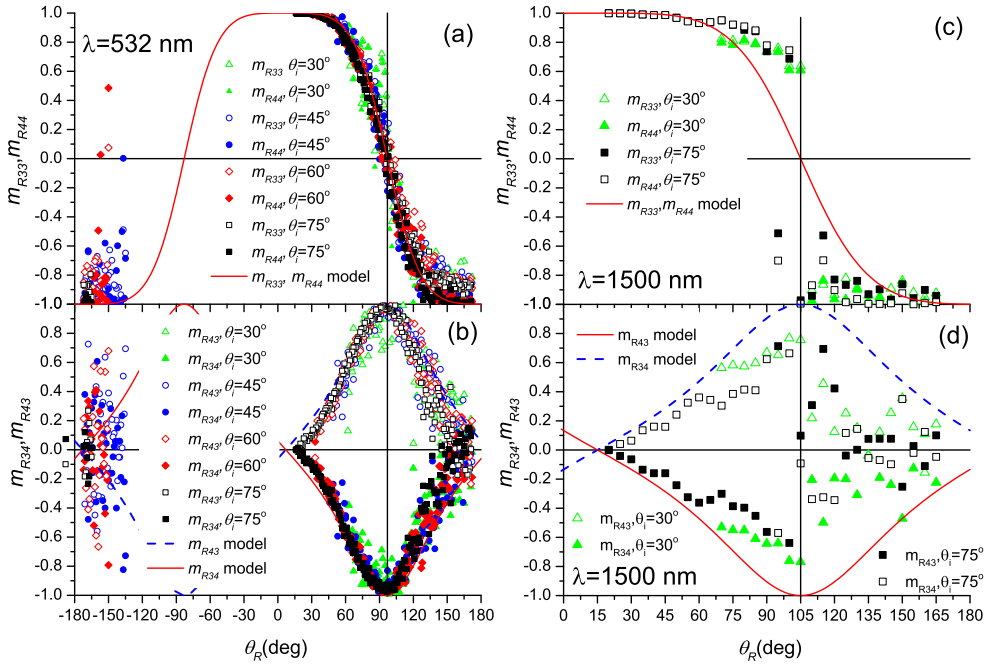

Fig. 7. Figures (a) at 532 nm and (c) at 1500 nm show the m_{R33} and m_{R44} elements from the retardance matrix $\mathbf{M}_R$ plotted against the Rayleigh scattering angle θ_R. The simulated curve is given by Rayleigh scattering theory (see Eq. (14)). Figs. (b) at 532 nm and (d) at 1500 nm show the m_{R34} and m_{R43} elements from the retardance matrix $\mathbf{M}_R$ plotted against θ_R. The simulated curve shows $\pm S$ (see Eq. (15)). The left Figs. (a) and (b) are data at 532 nm, with incident angles $\theta_i = 30°, 45°, 60°, 75°$. The simulated data at 532 nm (full and dotted lines) use $\theta_B \approx 7°$. Figs. (c) and (d) are data at 1500 nm, with incidence angles $\theta_i = 30°$ and $75°$, and simulated data with $\theta_B \approx 15°$. The vertical lines indicate the location of θ_B.

Having determined the basic functional forms for the lower right elements of the $\mathbf{m}_R$ retardance sub-matrix, we may similarly try to parametrize the remaining elements of $\mathbf{m}_R$, see the experimental data in Fig. 8. Indeed, the function $-0.02 + 0.17R \approx -p_0/3 + R/6$, where $R = \arccos(C)$, gives a reasonable fit to the available data sets at 532 nm, for the m_{R23} element (note that m_{Rij} refers to the retardance matrix M_R). Similarly, the function $0.02 - 0.23N \approx p_0/3 - N/4$ fits the m_{R24} dataset, while $m_{R22} \approx 1$. Adapting the symmetries $m_{R23} \approx m_{R32}$ and $m_{R24} \approx -m_{R42}$, we obtain a reasonable model for the entire retardance sub-matrix. The experimental decomposed retardance sub-matrix at 532 nm and incidence angles $\theta_i = 30°$, $45°$, $60°$ and $75°$ is shown together with the simulations in Fig. 8. This model for the retardance sub-matrix appears reasonable, and a similar model also appears suitable at 1500 nm.

There are other interesting features in the diattenuation and the polarizance vectors, particularly in the m_{12} and m_{21} elements, of the original measured Mueller matrix, which appear to scale as $p_D^2 \approx \alpha^2$. Upon searching for the Rayleigh type functional form for the m_{12} and m_{21}

#188283 - $15.00 USD Received 11 Apr 2013; revised 11 Jul 2013; accepted 11 Jul 2013; published 26 Jul 2013

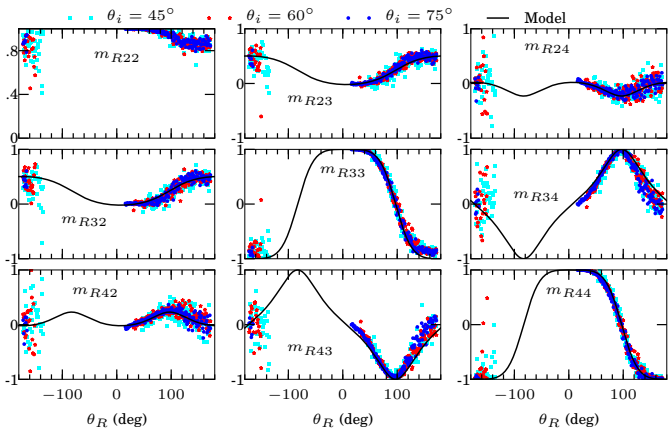

Fig. 8. The experimental retardance sub-matrix $\mathbf{m}_R$ (symbols) and the simulated $\mathbf{m}_R$ (full lines), both plotted against the Rayleigh scattering angle θ_R. The experimental data are at 532 nm, with incident angles $\theta_i = 30°$, $45°$, $60°$ and $75°$. The simulated data use $\theta_B \approx 7°$, and the basis functions N, C and S in addition to p_0. The notation m_{Rij} refers to the retardance matrix M_R.

elements, it was observed that

$$\frac{m_{12} + p_0/2}{4p_D^2} \approx -\frac{\sin^2(\theta_R - \theta_B)}{1 + \cos^2(\theta_R - \theta_B)} = -N. \tag{16}$$

The offset angle θ_B is found to be similar, although not identical, to the corresponding angle for the retardance matrix. Although both N, S and C appear as reasonable functional forms to describe the full data sets, there are certain problems with the periodicity of these functions as a function of θ_R. We therefore believe that a further improved model must properly include other nonlinear effects in both θ_R and θ_B as a result of refraction, and thus as a function of incidence and the Rayleigh scattering angle. Finally, it is noted that the diattenuation sub-matrix was found to be close to the identity matrix, and any variations therein was neglected in the development of the parametric model.

4.4. Final parametric model for the Mueller matrix at 532 and 1500 nm

We now return to the original Mueller matrix, and seek a parametric model using the functional forms based on α, β and γ, in addition to N, C and S as determined in the above decomposition analysis. We propose that a simplified parametric model for the Mueller matrix for the Spectralon, can now be obtained using polar product decomposition. First, let $\mathbf{p} \approx \mathbf{d} \approx \left[\frac{1}{2}p_0 - 4\alpha^2 N, 0, 0\right]^T$, $\mathbf{m}_\Delta \approx \text{diag}(\alpha,\beta,\gamma)$, $\mathbf{m}_D \approx \text{diag}(1,1,1)$ and $\mathbf{m}_R \approx \begin{bmatrix} 0 & 0 & 0 \\ 0 & C & S \\ 0 & -S & C \end{bmatrix}$, giving the $\mathbf{M}_\Delta$, $\mathbf{M}_R$ and $\mathbf{M}_D$ matrices in Eq. (2). A direct application of the forward decomposition, i.e. using Eq. (1), will lead to additional terms of the order $\alpha|\mathbf{d}|$, $|\mathbf{d}|^2$ and smaller, and further $\mathbf{p}$ is no longer identical to $\mathbf{d}$ as initially assumed. This is an artefact due to the simplifications in the parametrisation of the decomposed matrices. We therefore argue that the observed symmetry of the experimental Mueller matrix must remain, and that the Mueller matrix should also remain physically realizable in the forward scattering direction. As a result, these additional terms can be neglected. The latter approximation gives identical results to simply letting $\mathbf{p} = \mathbf{0}$ in $\mathbf{M}_\Delta$, prior to the matrix multiplication, and a back-substitution of $\mathbf{p} = \mathbf{d}$ into the final Mueller

#188283 - $15.00 USD Received 11 Apr 2013; revised 11 Jul 2013; accepted 11 Jul 2013; published 26 Jul 2013

matrix. The latter approach will result in the following simplified Mueller matrix with a certain physical basis

$$\mathbf{M} \approx M_{11} \begin{bmatrix} 1 & \frac{1}{2}p_0 - 4\alpha^2 N & 0 & 0 \\ \frac{1}{2}p_0 - 4\alpha^2 N & \alpha & 0 & 0 \\ 0 & 0 & \beta C & \beta S \\ 0 & 0 & -\gamma S & \gamma C \end{bmatrix}, \tag{17}$$

where C, S and N are defined as in Eqs. (14), (15) and (16), respectively. We similarly propose a complete parametric model using the above basis functions, that will better fit also the off diagonal elements of the Spectralon Mueller matrices. From trial an error, we parametrize $\mathbf{p} \approx \mathbf{d} \approx \left[\frac{1}{2}p_0 - 4\alpha^2 N, \frac{1}{2}p_0 - 2\alpha^2 N, \frac{1}{3}p_0\right]^T$. We use $\mathbf{m}_\Delta \approx \mathrm{diag}(\alpha,\beta,\gamma)$ and $\mathbf{m}_D \approx \mathrm{diag}(1,1,1)$ as above, while the retardance sub-matrix is refined to

$$\mathbf{m}_R \approx \begin{bmatrix} 1 & -\frac{1}{3}p_0 + \frac{R}{6} & \frac{1}{3}p_0 - \frac{1}{2}N\sin\chi \\ -\frac{1}{3}p_0 + \frac{R}{6} & C & S \\ -\frac{1}{3}p_0 + \frac{1}{2}N\sin\chi & -S & C \end{bmatrix}, \tag{18}$$

where $R = \arccos(C)$. Furthermore, the oscillation of the m_{24} and the $-m_{42}$ elements have been introduced in the model as a function of χ. Hence, the matrix product of Eq. (1), with $\mathbf{p} = \mathbf{0}$, followed with a back-substitution of $\mathbf{p} = \mathbf{d}$ in the resulting Mueller matrix, result in the following Mueller matrix

$$\mathbf{M} = M_{11} \begin{bmatrix} 1 & \frac{1}{2}p_0 - 4\alpha^2 N & \frac{1}{2}p_0 - 2\alpha^2 N & \frac{1}{3}p_0 \\ \frac{1}{2}p_0 - 4\alpha^2 N & \alpha & \alpha\left(\frac{1}{3}p_0 - \frac{1}{6}R\right) & \alpha\left(\frac{1}{3}p_0 - \frac{1}{2}N\sin\chi\right) \\ \frac{1}{2}p_0 - 2\alpha^2 N & \beta\left(\frac{1}{3}p_0 - \frac{1}{6}R\right) & \beta C & -\frac{1}{4}p_0 + \beta S \\ \frac{1}{3}p_0 & \gamma\left(-\frac{1}{3}p_0 + \frac{1}{2}N\sin\chi\right) & \frac{1}{4}p_0 - \gamma S & \gamma C \end{bmatrix}. \tag{19}$$

We get two sets of parameters, one for each wavelength. For 532 nm, the parameters for the depolarization factors are given in Table 1, with $\theta_B \approx 7^\circ$. For 1500 nm, the parameters for the depolarization factors are given in Table 2, and $\theta_B \approx 15^\circ$. Note that the m_{14} and m_{41} elements are negligible at 1500 nm, and that a small constant $\pm p0/4$ has been added to the m_{34} and m_{43} elements, for a minor adjustment to the experimental data. We have used $\chi = 30^\circ$ for the modelling of both wavelengths in Figs. 2 and 4. Similarly, one could propose a small, although more uncertain, oscillation in the m_{34} and m_{43} elements.

The Mueller matrix resulting from the parametric model in Eq. (19), is plotted in Fig. 2 together with the experimental data. It is observed, that there is a reasonable correspondence to the range of obtained experimental data. There is a distinct improvement in the correspondence between the model and the experimental results compared to previous work [1], although more parameters have been introduced in the new model. The modelled Mueller matrix for 1500 nm is shown in Fig. 4 together with the data at 532 nm. Only weak differences are observed between the two wavelengths, e.g. m_{14} and m_{41} have a much smaller offset at 1500 nm, and m_{44} is larger at 1500 nm. A self consistency-check was performed by recalculating the polarization index p_D using Eq. (8) for both wavelengths. This recalculated polarization index was found to be in excellent agreement with both the experimental data and the Gaussian model in Eq. (11), except for the already mentioned deviation for scattering near parallel to the surface.

The parametric model indicate that Mie and Rayleigh scattering appears as an important process for the Spectralon reflectance standard. It is interesting that the complex form of the retardance matrix can be derived from the basis functions N, C and S. However, as with Rayleigh particles, little direct information about the particles themselves are projected in the current

#188283 - $15.00 USD Received 11 Apr 2013; revised 11 Jul 2013; accepted 11 Jul 2013; published 26 Jul 2013

model, except for possibly the shift angle θ_B, which may be regarded as a pseudo-Brewster angle, and thus be related to either the average material properties or the optical properties of the scatterers [30]. The apparent dispersion of θ_B supports the latter hypothesis. It is striking that the m_{12} and the m_{21} elements are apparently scaling with $\sim p_D^2$, possibly indicating a multiple scattering process. There are experimental uncertainties with respect to the constant offsets in the measured Mueller matrix (particularly m_{13} and m_{14}), but we have not been able to relate these to any evident experimental artefacts. As in [1], the m_{14} and m_{41} elements have been modelled by constants.

Finally, to reduce the number of free parameters, the result in Eq. (19) can be put into a reduced form

$$\mathbf{M} = M_{11} \begin{bmatrix} 1 & -4p_D^2N & -2p_D^2N & 0 \\ -4p_D^2N & p_D & -p_D\frac{1}{6}R & -p_D\frac{1}{2}N\sin\chi \\ -2p_D^2N & -p_D\frac{1}{6}R & p_DC & p_DS \\ 0 & p_D\frac{1}{2}N\sin\chi & -p_DS & p_DC \end{bmatrix}, \tag{20}$$

where $p_D \approx p_C \approx \alpha \approx \beta \approx \gamma$ and p_0 has been neglected. It is now clearly observed that the lower right 3×3 matrix is basically the retardance sub-matrix multiplied with the average depolarisation factor. To complete the discussion, we can now write the matrix as the sum of an ideal diffuser scaling with the average degree of depolarization, and a correction matrix scaling with the average degree of polarization

$$\mathbf{M} = M_{11} \left((1-p_D)\,\mathrm{diag}(1,0,0,0) + p_D \begin{bmatrix} 1 & -4p_DN & -2p_DN & 0 \\ -4p_DN & 1 & -\frac{1}{6}R & -\frac{1}{2}N\sin\chi \\ -2p_DN & -\frac{1}{6}R & C & S \\ 0 & \frac{1}{2}N\sin\chi & -S & C \end{bmatrix} \right), \tag{21}$$

i.e. in a similar form to the one previously reported [1], but with basis functions with an improved physical insight.

It appears interesting to study other well determined diffuse samples to investigate whether the above product decomposition method and in particular, the parametric model found for the Spectralon, may be applied to other strongly scattering systems, such as rough surfaces and powder samples. The exact dependency of incidence angle is expected to be revealed with a combination of more data and improved models. As a result, it is envisaged that more information about the scatterers may be extracted from the normalized Mueller matrix.

Preliminary studies of the current dataset, comparing the product decomposition and the current formulation of the differential decomposition [12, 16], give highly similar results for α, β, γ and the linear retardance in the range $0 \le \theta_R \le 90^\circ$, while it is interesting to observe that the current formulation of the differential decomposition method must be revised for $\theta_R > 90^\circ$. Indeed, this is as expected since the current form of the differential decomposition is only valid for forward scattering. A revised version of the differential decomposition method [12,16] could be a more appropriate tool for analysis of the scattering Mueller matrix for the Spectralon.

Finally, it has been proposed to further refine/validate the parametric model for the off-diagonal elements using a few higher order terms in the actual Mie solution. This approach would definitively result in a model based on stronger physical ground, but is out of the scope of the current work.

5. Conclusion

A new parametric model for the Mueller matrix of a Spectralon white reflectance standard diffuser has been determined through the use of polar (product) decomposition techniques. New

#188283 - $15.00 USD Received 11 Apr 2013; revised 11 Jul 2013; accepted 11 Jul 2013; published 26 Jul 2013

Mueller matrix data at the wavelengths 532 nm and 1500 nm are presented and analyzed. It was found particularly useful to study the Spectralon in terms of the standard ”particle” or Rayleigh scattering angle, which made the depolarization index and the Mueller matrix elements close to independent of the incidence angle. The basic building blocks in the new model is a Gaussian parametric model for the depolarization index, multiplied with Rayleigh like functional forms deduced from the decomposed matrices. A pseudo Brewster angle appeared dispersive and characteristic of the material. The use of decomposition techniques appears promising in order to reveal the basic functional building blocks of a given scattering Mueller matrix, and it is envisaged that the methodology presented here can be used to study other strongly diffuse samples. Finally, a well characterized Mueller matrix of the Spectralon makes it also useful as a calibration standard for polarization sensitive systems.

Acknowledgment

L.M.S. Aas and J. Maria acknowledge support from The Norwegian Research Center for Solar Cell Technology (project num. 193829).

#188283 - $15.00 USD Received 11 Apr 2013; revised 11 Jul 2013; accepted 11 Jul 2013; published 26 Jul 2013